Naval Research Laboratory
Washington, DC 20375-5320

NRL/7350/FR--2022/3

Quantifying the Frequency With Which Visual Signatures in Time-Averaged Imagery Indicate the Location of a Rip Channel

SARAH TRIMBLE
ALLISON PENKO

Seafloor Sciences Branch
Ocean Sciences Division

October 24, 2022

REPORT DOCUMENTATION PAGE

PLEASE DO NOT RETURN YOUR FORM TO THE ABOVE ORGANIZATION

1. REPORT DATE	2. REPORT TYPE	3. DATES COVERED	
		START DATE	END DATE
October 24, 2022	NRL formal report	October 1, 2019	August 8, 2022

4. TITLE AND SUBTITLE

Quantifying the Frequency With Which Visual Signatures in Time-Averaged Imagery Indicate the Location of a Rip Channel

5a. CONTRACT NUMBER	5b. GRANT NUMBER	5c. PROGRAM ELEMENT NUMBER
		0601153N
5d. PROJECT NUMBER	**5e. TASK NUMBER**	**5f. WORK UNIT NUMBER**
		1R32

6. AUTHOR(S)

Sarah Trimble and Allison Penko

7. PERFORMING ORGANIZATION / AFFILIATION NAME(S) AND ADDRESS(ES)	8. PERFORMING ORGANIZATION REPORT NUMBER
U.S. Naval Research Laboratory 4555 Overlook Ave. SW, Washington, DC 20375-5320	NRL/7350/FR--2022/3

9. SPONSORING / MONITORING AGENCY NAME(S) AND ADDRESS(ES)	10. SPONSOR / MONITOR'S ACRONYM(S) NUMBER	11. SPONSOR / MONITOR'S REPORT NUMBER(S)
Office of Naval Research 875 N. Randolph Street, Suite 1425 Arlington, VA 22203-1995	ONR	

12. DISTRIBUTION / AVAILABILITY STATEMENT

Distribution Statement A. Approved for public release: distribution unlimited.

13. SUPPLEMENTAL NOTES

14. ABSTRACT

15. SUBJECT TERMS

16. SECURITY CLASSIFICATION OF:			17. LIMITATION OF ABSTRACT	18. NUMBER OF PAGES
a. REPORT	b. ABSTRACT	c. THIS PAGE		
UNCLASSIFIED	UNCLASSIFIED	UNCLASSIFIED	SAR	27

19a. NAME OF RESPONSIBLE PERSON	19b. PHONE NUMBER *(Include area code)*
Sarah Trimble	228-688-5671

This page intentionally left blank

CONTENTS

FIGURES

TABLES

QUANTIFYING THE FREQUENCY WITH WHICH VISUAL SIGNATURES IN TIME-AVERAGED IMAGERY INDICATE THE LOCATION OF A RIP CHANNEL

1. INTRODUCTION

Video cameras were first introduced as a low-cost, logistically accessible nearshore sensor in the late 1980s with the Argus system (Lippmann & Holman, 1989, 1990). Over the next 15 years, methods were developed that use these sensors to observe nearshore characteristics such as wave height (e.g.: Aarninkhof & Ruessink, 2004; Almar et al., 2012; Andriolo, 2019 and others), run-up (Holman & Guza, 1984; Simarro et al., 2015), celerity (Holland et al., 1991), and surface currents (Chickadel, 2003). Methods have also been developed to estimate locations of wave breaking from observations (e.g., Piotrowski & Dugan, 2002; Simarro et al., 2019; Stockdon & Holman, 2000; Thuan et al., 2019 and others). Today, video cameras remain a popular nearshore observation tool because they are relatively inexpensive and logistically simple to set up on site, and they can be used to observe a site continuously throughout daylight hours (Holman & Stanley, 2007).

One product of these sensors is a time-averaged image, also called time exposure, or timex, imagery, created by averaging 10 minutes of frames captured at 1 or 2 Hz (Holman & Stanley, 2007). These images can indicate where waves are interacting with the crest of a sandbar, causing them to break and to generate white surface foam. This foam is recorded in the RGB time averaged image as higher-intensity pixels (greater than 200 on an 8-bit scale of 0–255; examples shown in Figs. 1b, 1c, 1d, and 5). Dimensionless pixel intensity values (0–255) cannot be converted into bathymetric elevations (0–∞), but there is evidence that local maxima in pixel values spatially correspond with local maxima in bathymetric elevations under specific environmental conditions (Holman et al., 2013; Simarro et al., 2019; Thuan et al., 2019; Figure 1a and 1b). As a result, it is possible to track the location of wave breaking using timex imagery and that location is often interpreted as the location of the sandbar (Guedes et al., 2011; Mallet et al., 2000; Pape et al., 2010; Ruessink et al., 2009).

A similar spatial correspondence may exist between the local minima in pixel intensity and local minima in wave breaking (Bruneau et al., 2009; Holman et al., 2006; MacMahan et al., 2005). The decrease in wave breaking may be caused by: (a) lower bathymetric elevations, (b) the offshore-directed flow of a rip current, or (c) both. The interaction of alongshore variations in coastal morphology and incident wave angles creates variations in wave height and wave breaking alongshore, where areas with higher waves and more intense breaking that generate increased set-up (high-intensity pixels) are adjacent to areas of lower wave heights, less breaking, and less set-up (low-intensity pixels). In addition, the adjacent regions of high and low set-up can generate a pressure gradient that can cause the focused, offshore-directed flow of a rip current (Castelle et al., 2016; Haller, 2002). Both a rip channel and/or a rip current may cause the decreased wave breaking that is apparent in timex imagery but to date, no study has quantified whether either cause is consistent.

Manuscript approved October 17, 2022.

1.1 Background

Figure 1 is a timeline of the pioneering efforts in utilizing pixel intensity recorded in timex imagery to estimate the location of local maxima and minima in nearshore bathymetry. Early publications compared cross-shore transects of timex image pixel intensity to cross-shore transects of field-surveyed bathymetry and showed that qualitatively, both values peaked in similar cross-shore locations (Lippmann & Holman, 1989, 1990; Fig. 1a). Multiple publications through the 1990s used transects of timex images to track the cross-shore position of wave breaking, which they interpreted as the cross-shore position of the sandbar crest (e.g., Konicki & Holman, 2000; Lippmann & Holman, 1989; Ruessink et al., 2000; van Enckevort & Ruessink, 2001; and many others). For a comprehensive review of studies tracking local maximum elevations with video imagery, see Román-Rivera and Ellis (2019).

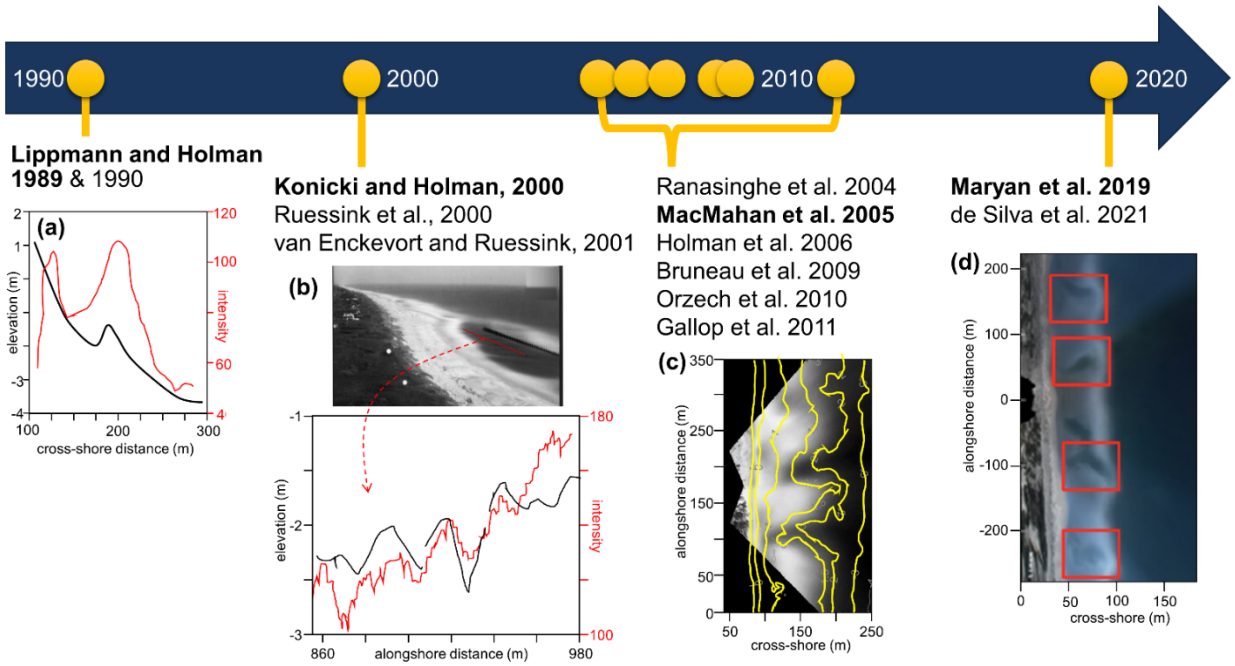

Fig. 1—Examples of research developments using timex imagery to track areas of wave breaking (and lack thereof). Bold citations indicate the source of the adapted plot shown below. (a) The first papers to use video cameras for remotely observing the near shore showed that maximums of pixel intensity (red line) and elevation (black line) had spatial correspondence in 2D cross-shore transects. (b) Following studies showed spatial correspondence may exist in alongshore transects between local minimums of pixel intensity and local minimums of elevation; note that the intensity profile (red) is not from the exact location as the elevation profile (black). (c) Qualitative spatial correspondence was observed between visual signatures (background grayscale) and shore-normal channels observed in bathymetry (yellow contour lines). (d) Machine learning methods can automate the detection and digitization of visual signatures (red boxes) in timex images (background image) with a 98% accuracy rate.

In the early 2000s, accessible survey technology progressed beyond transects, and comparisons of spatially dense bathymetric surveys to timex imagery revealed that higher elevations and higher-intensity pixels could be spatially correspondent not only in cross-shore transects but also throughout an image (Konicki & Holman, 2000; Ruessink et al., 2000; van Enckevort & Ruessink, 2001). In 2003, Holman et al. were the first to suggest that spatial correspondence between local maxima in wave breaking and pixel intensity implied a matching spatial correspondence between local minima in wave breaking and pixel intensity. Panels C and D in Fig. 1 show how a region of relatively low-intensity pixels can appear as a narrow, shore-normal feature intersecting the regions of high-intensity pixels resulting from breaking waves (see also Fig. 5). Throughout the remainder of this paper, the term “visual signature” is used to refer to this

shore-normal region of low-intensity pixels intersecting the high-intensity pixels of the surf zone in timex imagery. A number of studies have used the visual signature to track the alongshore location of flowing rip currents (Holman et al., 2006) and rip channels (Gallop et al., 2011; Orzech et al., 2010; Quartel, 2009; Splinter et al., 2011). Yet, while Holman et al. (2003) includes a comprehensive review of supporting observations prior to that publication date, it does not contain quantitative analysis of pixel intensity and bathymetric observations or observations of rip current flow. Ranasinghe et al. (2004) is often cited as the pioneering evidence that a reliable spatial correspondence exists between visual signatures and rip channels. However, they validated rip channel presence with a threshold 70% agreement between human digitizers of timex images and did not include analysis of bathymetric observations.

Multiple field campaigns have collected timex imagery and bathymetric observations showing spatial correspondence can exist between visual signatures and rip channels (Bruneau et al., 2009; MacMahan et al., 2005; Moulton et al., 2017b) as well as rip flow (MacMahan et al., 2005; Moulton et al., 2017a; Fig. 1c). However, no study has yet quantified how often the visual signature correctly (or incorrectly) indicates the presence of a rip channel or an actively flowing rip current. Despite this lack of quantified uncertainty, two recent papers have used machine learning and deep learning methods to automate the identification of visual signatures. Automation removes the subjective human digitization of visual signatures, and again interprets the location of a lack of wave breaking as indicating either a rip channel (Maryan et al., 2019) or a rip current (de Silva et al., 2021). Both papers achieved a 98% accuracy rate for identifying visual signatures in imagery (de Silva et al., 2021; Maryan et al., 2019) and video (de Silva et al., 2021). However, neither paper made assertions as to the reliability of an identified visual signature accurately indicating the location of either a rip channel or a flowing rip current.

1.2 Motivation

The present body of literature has established the following: (1) high-intensity pixels in cross-shore transects of timex imagery are spatially correspondent with areas of increased wave breaking and higher elevations (Lippmann and Holman, 1990, 1989), (2) low-intensity pixels in alongshore transects can be spatially correspondent with rip channels and rip currents (Konicki and Holman, 2000; Ruessink et al., 2000; van Enckevort and Ruessink, 2001) but the reliability of that spatial correspondence is unknown, and (3) machine learning methods can be used to reliably identify narrow, shore-normal regions of low-intensity pixels in timex images (Maryan et al., 2019) and satellite images and video (de Silva et al., 2021). In addition, published works have hypothesized that the decreased wave breaking that generates the visual signature may be the result of either (1) lowered elevations within a rip channel, (2) an actively flowing rip current, or (3) both. At present, there is rapid progress in research utilizing imagery to remotely track rip channels and potential rip currents. However, to progress this line of research, it is necessary to quantify the frequency with which a visual signature indicates a rip channel. Future research can investigate how often the visual signature indicates the location of a flowing rip current.

Section 2 describes methods we employed. The precise and spatially dense bathymetric observations captured by lidar we used were not available to many previous studies in this body of literature. In addition, the automated method we utilized to objectively identify visual signatures has several advantages over digitization methods that are human-reliant and therefore subjective. Section 3 presents results and Section 4 discusses how results compare and contrast with previous work. Analysis in this paper is of one beach site on four dates, but methods are detailed so that repeat studies can investigate whether results transfer to other beaches and oceanographic conditions.

2. APPROACH

Our primary aim was to determine the frequency with which the presence of a visual signature recorded in timex images indicated the presence of a rip channel in the surf zone. The following subsection 2.1 describes the study site and field data collection. Subsection 2.2 describes the definition of a rip channel, and subsection 2.3 describes the definition of a visual signature. Subsection 2.4 describes the methods employed to calculate the spatial and temporal correspondence between those features. Subsection 2.5 describes analysis of the influence of wind and wave conditions on the results. A final subsection 2.6 summarizes the overall workflow.

2.1 Field Observations

All imagery and field measurements of bathymetry, wind, and waves were collected at the United States Army Corps of Engineers' (USACE), Field Research Facility (FRF) and Coastal Hydraulics Lab (CHL) located in Duck, North Carolina, USA (Fig. 2). Bathymetric observations were from four lidar data sets provided by the National Oceanic and Atmospheric Association (NOAA) Office for Coastal Management (OCM). Each lidar survey was processed into a digital elevation model (DEM) by averaging observations into an output cell size 4 to 5 times the average point spacing of observations, per the industry standard. The resulting DEMs had horizontal resolutions of 5 m (2013-10-02 and 2015-10-31), 1.35 m (2016-07-02), and 3 m (2019-06-19). The GPS times recorded in the raw files show that each survey was collected within a 4-hour window. These DEMs represented various stages of the intermediate beach morphologies described by Wright and Short (1984) and were representative of the study site.

Surf zone imagery was obtained from an array of cameras, mounted on a tower recording RGB images at 2 Hz. Each timex image was created by averaging 1,200 frames collected by the cameras over 10 minutes at the top of every daylight hour. These timex images were retrieved from the archives of the Coastal Imaging Lab (CIL) at Oregon State University (OSU) and were georectified into real-world coordinates. Only images collected within ±12 hours of the lidar bathymetric observations were used. Images cover a 1.5-km stretch of beach at the site. Over- or underexposed images were removed from analysis and portions of images affected by camera malfunctions were masked from the analysis. The resulting dataset consisted of 51 viable images over four days.

Wind observations were sampled by an R.M. Young marine anemometer mounted at the end of the FRF pier, 19.36 m above sea level. Reported wind speeds and directions were vector averaged at 1 Hz over the 10-min sampling period. Water levels were sampled every 6 minutes by a NOAA tide station (ID#8651370) located at the end of the FRF pier. Wave data were sampled hourly by a bottom-mounted, upward-looking Nortek AWAC at 6 m depth. The locations of these instruments are shown in Fig. 2c.

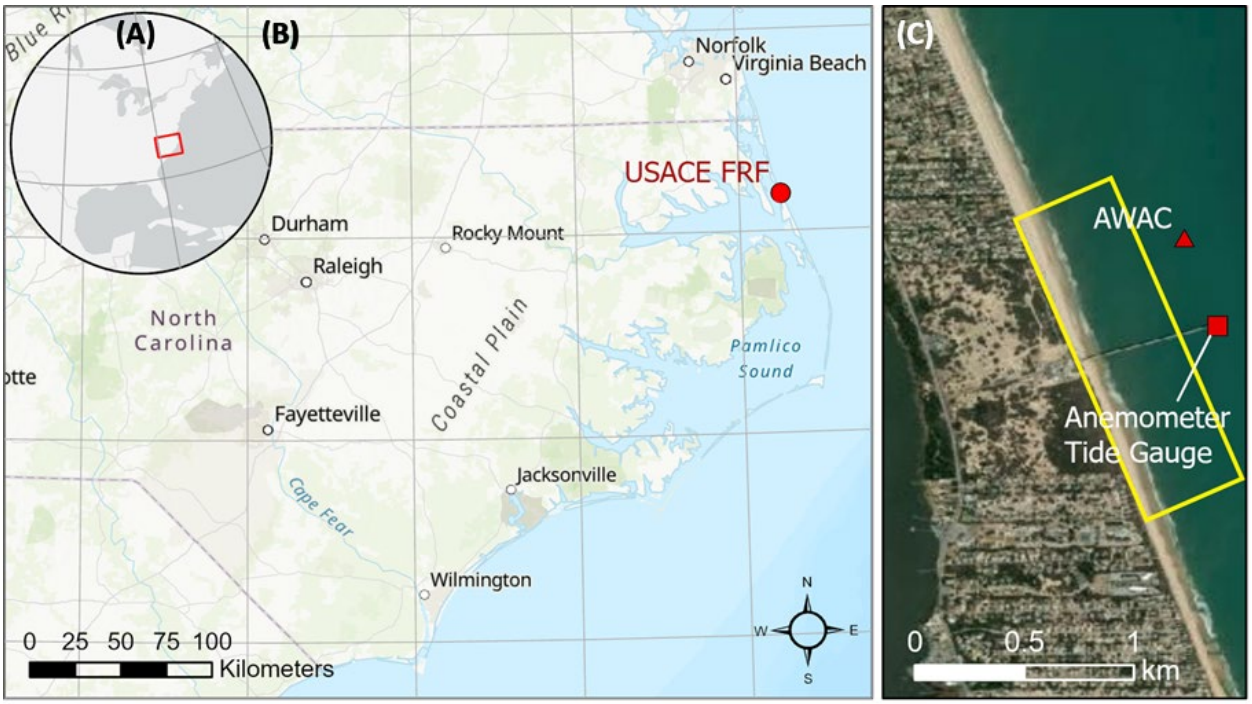

Fig. 2—The location of the USACE FRF in Duck, North Carolina, USA. (A) Circle inset map at the upper left shows the eastern United States, with a red box indicating the extent of (B) the map of coastal North Carolina. The FRF is located on the northern Outer Banks barrier island chain of North Carolina. Panel (C) shows satellite imagery of the FRF, the footprint of timex images used (yellow outline) and locations of field instruments (red symbols). Data used for this figure are courtesy of Esri, USGS, GeoEye, and the State of North Carolina Department of Transportation.

2.2 Defining Rip Channels

In most rip current studies, the morphology of rip channels is described qualitatively, if it is described at all. The exception is Brander and Cowell (2003), who provide the following detailed morphometric definition: rip channel width is variable because channel cross-section shape can vary widely, channel length is typically 1–2 times the width of the surf zone, and channel depth is the vertical distance from mean water level to the thalweg. In general, rip channels have a relief ≥ 1 m from surrounding morphology. Velocities are faster in narrower channels with constrained cross-sectional area, and/or greater relief (Brander, 1999).

We systematically identified locations of rip channels in the lidar-derived DEMs following the methods of Brander and Cowell (2003) and utilizing a Geographic Information System (GIS). For each of the four lidar data sets, a fifth-order polynomial trend was calculated from all elevations between the shoreline (0 m) and a 150-m Euclidean distance in the offshore direction. Subtracting the DEM from that trend surface identified all regions in the nearshore bathymetry that comprised elevations below the trend, hereafter called "bathymetric depressions." These bathymetric depressions were further analyzed to determine if they were sufficiently narrow and shore-normal to represent potential rip channels. A bathymetric depression was labeled as a rip channel when the ratio of its maximum offshore extent to its maximum alongshore extent was >1.0 and if the longest axis across it was perpendicular to shore (±45°). Rip channels are therefore a subset of the regions labeled as bathymetric depressions. Figure 3 shows a vertically exaggerated 3D rendering of a DEM with both bathymetric depressions and rip channels outlined.

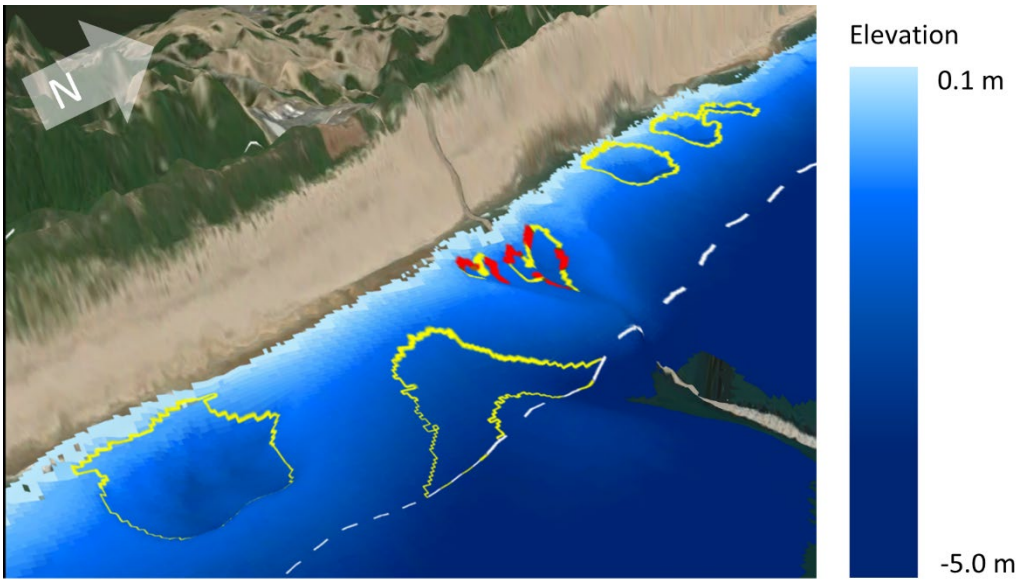

Fig. 3—A 3-D extruded graphic of part of the DEM for 2019-06-19. Satellite imagery has been draped over elevations above the 0-m contour. The increasingly saturated blue pixels are DEM elevations in the near shore (see color bar at right). Bathymetric depressions identified by de-trending are outlined in yellow. Two bathymetric depressions at the center (marked with a red-and-yellow dash) also meet the definition of a rip channel. The dashed, white line shows the seaward boundary of the area analyzed, a 150-m buffer from the shoreline.

2.3 Defining Visual Signatures

Previous research in this field relied on human-aided digitization of visual signatures in timex images (e.g.: Holman et al., 2006; Ruessink et al., 2000; Splinter et al., 2011). The common practice is to use a team of human digitizers to outline visual signatures in the image set, then to use a threshold agreement to finalize visual signature location (e.g., 70% agreement among digitizers; see Ranasinghe et al., 2004). To reduce subjectivity, we automated the identification of visual signatures using a trained machine learner to identify visual signatures. The machine learner we used was developed by Maryan et al. (2019) when they evaluated 17 different algorithms for accuracy in identifying the visual signature. The tested algorithms included support vector machines, convoluted neural networks, and the object classifier used here: a Viola-Jones cascade with a meta-classifier backend (Ada-Boost). In their evaluation, Maryan et al. (2019) determined that this algorithm can identify visual signatures with 98% recall. It had the highest accuracy of those tested for identifying the low-intensity pixel value, narrow, and shore-normal visual signatures.

The meta-classifier was trained with 102 images containing 514 examples of visual signatures at our study site of Duck, North Carolina, USA, as well as images of Secret Harbour, WA, Australia. The input to the trained object classifier is a single band (blue) of the timex image, where pixel values are the intensity (0–255). It utilizes a cascade of Haar features to determine if a segmented version of the pixel space is a sufficient match for a narrow, shore-normal pattern indicative of the target. The output is the RGB version of the input timex image with the addition of red boxes around each identified visual signature. Hereafter, those red boxes are referred to as an object ID (examples shown in both Fig. 1d and Fig. 4a). For more details on the object classifier, its training, and evaluation, see Maryan et al. (2019).

2.4 Calculating Spatial Correspondence

Our aim was to calculate the frequency with which a visual signature was spatially correspondent to rip channels in observed bathymetry. Spatial correspondence was determined in a GIS by a threshold minimum 19.6% overlap between the visual signatures and rip channels. Rip channels were digitized as the outline produced by the de-trending methods described in Section 2.2 (examples shown in Fig. 3). Visual signatures were digitized as the rectangular object ID produced by the object classifier described in Section 2.3 (examples shown in both Fig. 1d and Fig. 4a). The threshold for spatial correspondence between a visual signature and rip channel was a ≥19.6% overlap of an object ID area with a rip channel. This value represents the percentage of a rectangular object ID that would overlap with an idealized ellipsoid rip channel if 50.1% of that ellipsoid were within the object ID and the longest axes of both features were of similar size. Each visual signature was classified as either a true positive or a false positive by whether that object ID had sufficient or insufficient overlap with a rip channel, respectively. A false negative occurred when a rip channel did not have 50.1% of its area within an object ID. Figure 4 shows one timex image that contained examples of all possible outcomes (true positive, false positive, and false negative). Outcomes were then used to calculate recall and precision, where:

$$Recall = \frac{True\ Positives}{True\ Positives + False\ Negatives}$$

$$Precision = \frac{True\ Positives}{True\ Positives + False\ Positives}$$

Recall reveals the percentage of rip channels that were indicated by visual signatures. Precision reveals the percentage of visual signatures that indicated a rip channel. For both ratios, values closer to 1.0 indicate better spatial correspondence and an increased likelihood that the visual signature is a reliable indicator of a rip channel. In the event that our definition of a rip channel was too restrictive, we then repeated these analyses to determine the frequency of spatial correspondence between visual signatures and the set of all bathymetric depressions, which were identified by the de-trending process but had no restrictions on shape or orientation.

True positive, false positive, and false negative outcomes were tallied by both count and by area. In this study, it was considered critical to summarize results by how often the outcomes occurred, as well as summarizing how much cumulative nearshore area was correctly or incorrectly indicated by the visual signatures. Because we utilized a GIS, we were able to tabulate both (a) counts of how many visual signatures resulted into the true positive, false positive, and false negative outcomes and (b) the cumulative area in square meters of each outcome (Table 1). In summary, recall and precision were calculated to analyze four possible definitions of spatial correspondence:

- rip channels as the target feature, with recall and precision tallied by the cumulative count of visual signatures classified into each outcome: true positive, false positive, and false negative,
- rip channels as the target feature, with recall and precision tallied by the cumulative area within each outcome,
- all bathymetric depressions as the target feature, with statistics tallied by count, and
- all bathymetric depressions as the target feature, with statistics tallied by area.

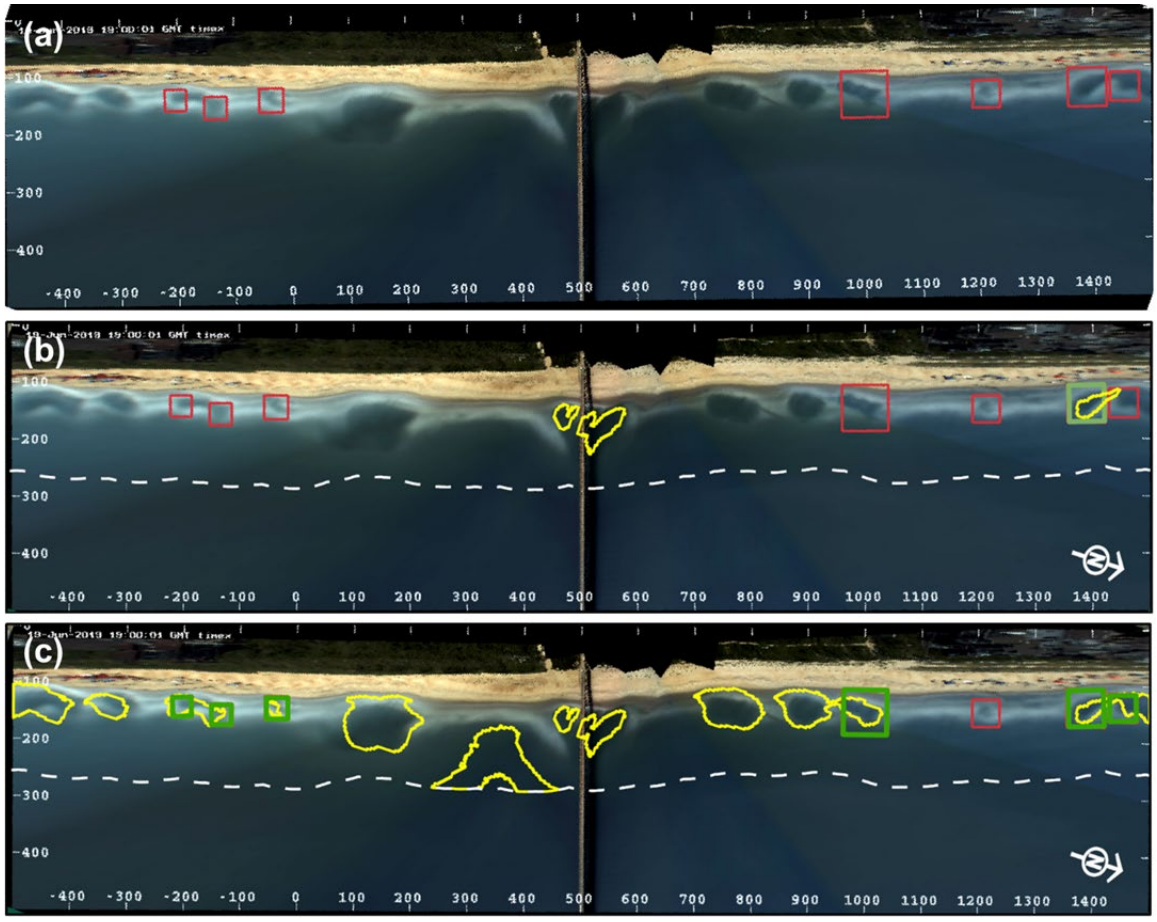

Fig. 4—The background in all three panels above is an RGB timex image from 1500 EDT on 2019-06-19 that resulted in all possible outcomes. The seaward boundary of the area analyzed was a 150-m Euclidean distance from shore (dotted, white line in panels b and c). (a) The output of the object identifier shows seven visual signatures in this image (red boxes). (b) The same output with the locations of three rip channels present in the DEM for this date. Two rip channels near the pier (yellow outlines) are false negatives because they are not indicated by a visual signature. At the northern end of the beach, one visual signature (green box) is a true positive because it has spatial correspondence with a rip channel. The remaining visual signatures are false positives (red boxes). (c) When analysis was extended to all bathymetric depressions present in the DEM for this date (yellow outlines), six of the seven visual signatures became true positives (green boxes). One visual signature remained a false positive (red box) but many of the bathymetric depressions were false negatives (yellow outlines).

Table 1—All Possible Outcomes of Spatial Correspondence Analysis

Outcome	Definition	By Count	By Area
True Positive	≥ 19.6% of the visual signature overlaps with a bathymetric feature.	Add 1 to cumulative sum of true positive cases.	Add the area of the object ID to the cumulative sum of true positive area.
False Positive	< 19.6% of the visual signature overlaps with a bathymetric feature.	Add 1 to cumulative sum of false positive cases.	Add the area of the object ID to the cumulative sum of false positive area.
False Negative	< 50% of a bathymetric feature overlaps with the area of one or more visual signatures.	Add 1 to cumulative sum of false negative cases.	Add the area of the bathymetric feature to the cumulative sum of false negative area.

2.5 Calculating Correlations Between Conditions and Rates of Spatial Correspondence

Ten independent variables were used to characterize oceanographic conditions during each image, including wave length, wave height, wave period, wave steepness, incident wave direction (relative to shore-normal), cross-shore component of wind velocity, direction of the maximum wind vector (relative to shore-normal), and water level. In addition, two non-dimensional parameters were calculated using observations from DEMs and the AWAC. The Iribarren number (Ir), also called the surf similarity parameter, quantifies the transition from non-breaking to breaking waves (Iribarren and Nogales, 1949),

$$Ir = \frac{\tan\beta}{\sqrt{H/_L}},$$

where H is wave height, L is wavelength, and β is the beach slope, calculated as the shortest Euclidean distance from the depth and location of the AWAC to the DEMs' 0 m contour. The Ursell number (U) quantifies the relationship between wave conditions and water depth and is given by

$$U = \frac{H \cdot L^2}{h^3},$$

where h is the depth of the water column (Ursell, 1953). These dimensionless values are commonly used to characterize the relationship between waves and bathymetry, which is described by beach slope in the Iribarren number and by depth in the Ursell number.

Correlation statistics were calculated between oceanographic variables (summarized by the aforementioned 10 variables) and results (summarized by recall and precision) to determine the effect of oceanographic conditions on rates of spatial correspondence. Both Pearson and Spearman correlations were calculated because we did not have a priori knowledge that data would meet the assumptions of Pearson. Pearson correlation, often referred to as linear regression, reveals linear relationships and assumes data are normally distributed. However, the relationships between wave height, wind speed, and other data analyzed are often nonlinear. Therefore, Spearman correlation was also calculated because it reveals relationships that are monotonic even if they are not linear and does not have the normal distribution assumption.

2.6 Workflow

Figure 5 summarizes the workflow of Sections 2.1–2.5. Four lidar surveys of the study site were processed into DEMs. The DEMs were de-trended, which digitized all bathymetric depressions. From this group of all bathymetric depressions, those that were narrow and shore-normal were labeled rip channels. All viable timex images from within 24 hours of each lidar survey were acquired from the archives hosted by the OSU CIL. The images were run through the object identifier to digitize the visual signatures. The counts and areas of true positive, false positive, and false negative outcomes were then tallied to generate the recall and precision of a visual signature indicating rip channels (or all bathymetric depressions). Field observations of wind, wave, and water conditions during each image were acquired from the USACE CHL and two different correlation statistics were calculated to examine the influence of 10 oceanographic variables on spatial correspondence. Results are discussed in the following Section 3.

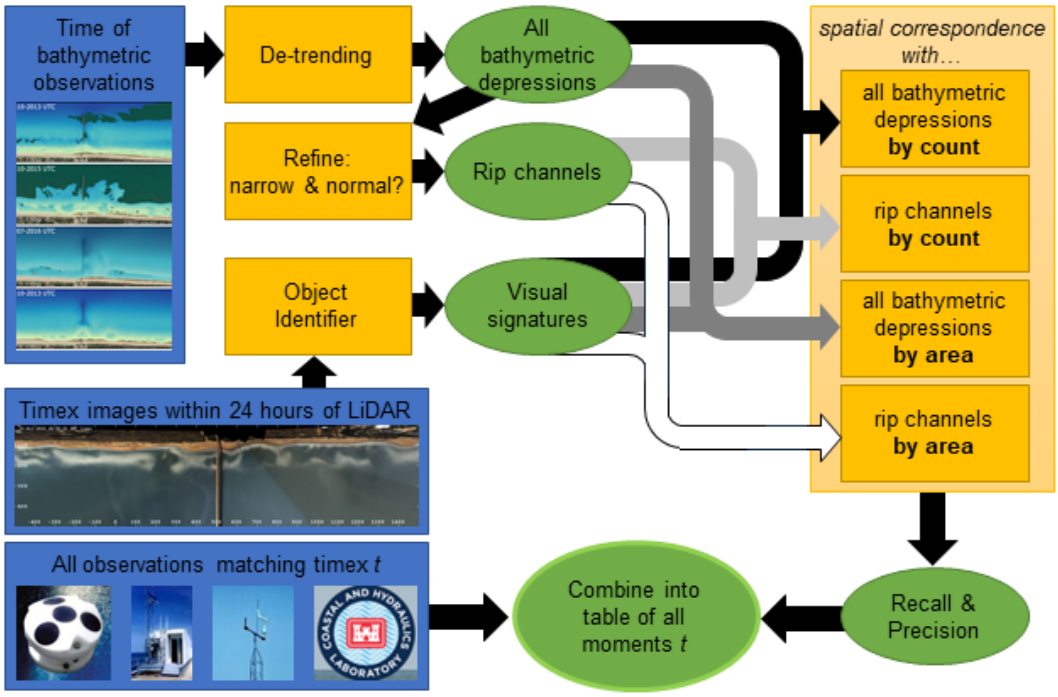

Fig. 5—Flow chart of the study methods. Blue boxes represent data sources, yellow boxes represent data processing, and green ovals represent outputs. The four overlapping arrows at the center represent the four comparisons between visual signatures and: (black arrow) all bathymetric depressions, using counts of outcomes; (dark gray) all bathymetric depressions by cumulative areas within outcomes; (light gray) rip channels by count; and (white) rip channels by area. These spatial correspondence outcomes were used to calculate recall and precision. The final output is a table with one record for each image (representing one moment in time t) including the 18 observations during t: the recall and precision for all 4 analyses of spatial correspondence and the 10 variables used to summarize oceanographic conditions at the time of that image.

3. RESULTS

Qualitative evidence shows that shore-normal regions of decreased wave breaking intersecting shore-parallel regions of breaking captured in timex imagery (i.e., visual signatures) can occur in the same space as rip channels (Gallop et al., 2011; Holman et al., 2003; Orzech et al., 2010; Quartel, 2009; Ranasinghe et al., 2004; Splinter et al., 2011). To quantify how often visual signatures indicate the presence of rip channels, we calculated spatial correspondence by both count and by area, as described in Section 2.4, Table 1, and Fig. 5. Precision and recall were calculated to determine whether visual signatures were consistently spatially correspondent with rip channels, and/or with the more generally defined group of all bathymetric depressions. Recall is the percentage of target features that are correctly indicated. Precision is the percentage of indications that are correct. Pearson and Spearman correlations were calculated to determine the effects of oceanographic conditions on precision and recall. Because qualitative evidence shows visual signatures can be correspondent with rip channels, it was expected that some spatial correspondence would exist between visual signatures and all bathymetric depressions, but that a higher correspondence would be observed with rip channels. However, these were not the results we observed.

3.1 Spatial Correspondence When Calculated by Count

There were 266 bathymetric depressions in these data (light-gray circle in Fig. 6a) and 51 of these were rip channels (dark-gray circle in Fig. 6a). The object identifier identified 98 visual signatures (dashed circle in Fig. 6a). Using the counts of true positive, false positive, and false negative outcomes to calculate

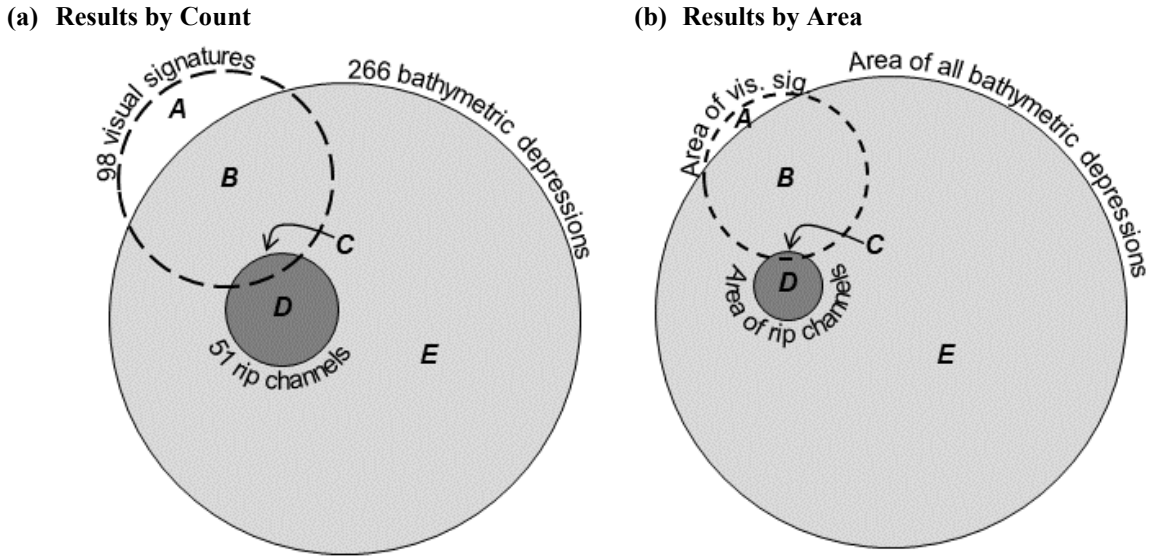

Fig. 6—(a) Venn diagram illustration of results when tallied by count. The dashed circle represents the 98 visual signatures present in the data. The large light grey circle represents the 266 bathymetric depressions, of which 51 were rip channels represented by the darker gray circle. (A) 20.4% of visual signatures were false negatives, existing outside all bathymetric depressions. (B) 79.6% of visual signatures were spatially correspondent to 7.9% of all bathymetric depressions. (C) 3.1% of visual signatures were true positive indicators of 3.9% of rip channels. (D) 96.1% of rip channels were not indicated by a visual signature. (E, inclusive of D) 92.1% of all bathymetric depressions were not indicated by a visual signature. (b) Venn diagram illustration of results when tallied by area. Overlap indicates the total space within features that exhibited spatial correspondence. The dashed circle represents the 0.46 km^2 within visual signatures. The large, light-gray circle represents the 3.75 km^2 with all bathymetric depressions, of which 0.08 km^2 was within rip channels (darker gray circle). (A) 7.2% of area within visual signatures was false negative, lacking spatial correspondence with any bathymetric depression. (B) 92.8% of visual signatures were spatially correspondent to 5.9% of all bathymetric depression area. (C) 3.1% of area within visual signatures was a true positive indicator of only 3.9% of rip channel area. (D) 96.1% of rip channel area was not indicated by a visual signature. (E, inclusive of D) 92.1% of all bathymetric depression area was false negative, not indicated by a visual signature.

recall and precision yielded low values for spatial correspondence between visual signatures and rip channels (5.77% and 3.06%, respectively). Values were higher for spatial correspondence between visual signatures and all bathymetric depressions (recall = 26.09%, precision = 79.59%). Only 20.4% of visual signatures were false positives (present outside of all bathymetric depressions; Fig. 6a area A). However, visual signatures were an unreliable indicator of both rip channel presence and of all bathymetric depressions in general. Only 3.1% of visual signatures were true positive indicators of a rip channel, and these indicated only 3.9% of the rip channels present (Fig. 6a area C). The vast majority of rip channels (96.1%) were false negatives not indicated by a visual signature (Fig. 6a area D). A higher 79.6% of visual signatures were true positive indicators of the more general group "all bathymetric depressions," but visual signatures indicated only 7.9% of all bathymetric depressions (Fig. 6a area B) with the vast majority (92.1%) of all bathymetric depressions labeled as false negatives because they were outside of visual signatures (Fig. 6a area E, inclusive of area D).

3.2 Spatial Correspondence When Calculated by Area

The cumulative area within all bathymetric depressions was 3.75 km^2 (light-gray circle in Fig. 6b) of which 0.08 km^2 was within rip channels (dark-gray circle in Fig. 6b). The object identifier identified a total 0.46 km^2 of visual signatures (dashed circle in Fig. 6b). Using the cumulative area of true positive, false positive, and false negative outcomes to calculate recall and precision yielded low values for visual signatures indicating the presence of a rip channel (11.03% and 2.10%, respectively). Recall for a visual

signature indicating the presence of any bathymetric depression was also low (10.71%), but precision was a high 92.80%. Although only 7.2% of area within visual signatures existed outside all bathymetric depressions (Fig. 6b area A), visual signatures indicated just 5.9% of the total area within all bathymetric depressions (Fig. 6b area B) and the vast majority (94.1%) of area within all bathymetric depressions existed outside of visual signatures (Fig. 6b area E, inclusive of area D). Visual signatures were also an unreliable indicator of rip channels. Just 2.1% of area within visual signatures indicated a meager 3.7% of the area within rip channels (Fig. 6b area C). The vast majority of rip channel area (96.3%) was not indicated by a visual signature (Fig. 6b area D).

3.3 The Effect of Evaluation Method on Results

Recall and precision had slightly different values when calculated by count and by area, for both rip channels and the more general group of all bathymetric depressions. To determine the effect of method (by count and by area) on these results, Pearson and Spearman correlations were calculated. The Pearson correlation reveals linear relationships, and the Spearman correlation can identify nonlinear monotonic relationships, where two variables may both increase (or both decrease) but at different rates. If the change in method (by count or by area) had no effect on the results, correlation between the recall and precision produced by the two different methods would be ~1.0.

Three of the four comparisons (Table 2) had R-squared values ≥0.86, indicating a strong correlation. The exception was a low Pearson correlation (R^2 =0.014) and a low Spearman correlation (R^2 =0.22) between the recall values for all bathymetric depressions produced by the two different methods. This weak correlation is the result of the large area of some bathymetric depressions. Unlike the formula for precision, the formula for recall (Eq. (1)) includes false negative outcomes. Therefore, if a single bathymetric depression (average size= 13,905.00 m^2) is classified as a false negative, the decrease in recall is larger for the area method than the comparative decrease in recall calculated by count, for the same observations. Recall for rip channels appears to be unaffected by this difference because rip channels were smaller (average size = 1,583.88 m^2) and because recall was extremely low whether calculated by count or by area (5.77% and 11.03%, respectively). Because recall for all bathymetric depressions was statistically affected by the difference in method (by count and by area), all results from both methods were retained throughout the course of this study and the remainder of this paper.

Table 2—Correlation Values (R^2) Between the Recall and Precision Calculated by Count and by Area for the Two Different Targets, All Bathymetric Depressions and Rip Channels

Rate	All Bathymetric Depressions		Rip channels	
	Pearson	Spearman	Pearson	Spearman
Precision	0.86	0.91	0.99	1.0
Recall	0.014	0.22	1.0	1.0

The weak correlation between the different recall values (for all bathymetric depressions, only) is highlighted in gray.

3.4 The Effect of Oceanographic Conditions on Results

Oceanographic conditions were summarized with 10 variables. The effect of oceanographic conditions on results was analyzed by evaluating those variables for correlation with precision and recall for the four comparisons seen in the center of Fig. 6 and listed at the end of Section 2.4. Precision reveals the proportion of all visual signatures that did have spatial correspondence with a target feature. Recall is the proportion of all target features that were indicated by a visual signature. For all correlations, relationships were considered significant when $R^2 \geq 0.60$ and $p \leq 0.05$, or possibly significant if $R^2 \geq 0.55$ and $p \leq 0.05$.

3.4.1 Pearson Correlations

When outcomes were tallied by count (top half of Fig. 7), there was a significant and negative linear correlation (-0.63) between the precision with which visual signatures indicated all bathymetric depressions and wave direction. In these data, larger values of the wave direction variable indicated increasingly oblique incident waves. Therefore, negative correlation indicates that increasingly oblique incident waves were associated with a decrease in precision. This condition decreases the likelihood that a visual signature will be a true positive. No other variables had significant linear correlation with recall or precision for either rip channels or the more general group of all bathymetric depressions.

When recall and precision were calculated from the cumulative area within outcomes (bottom half of Fig. 7), the precision with which visual signatures indicated all bathymetric depressions was significantly related to five oceanographic variables. Three variables were negatively correlated and two were positively correlated. As when tallied by count, decreased precision was correlated with increasingly oblique incident waves (-0.82). Decreased precision was also correlated with longer wave periods (-0.71) and longer wavelengths (-0.71). Under these conditions, visual signatures were more likely to be false positive indicators of a bathymetric depression. However, increased wave heights (0.71) and larger Iribarren numbers (0.80) were associated with increased precision. Under these conditions, there was an increased likelihood that visual signatures would be a true positive indicator of all bathymetric depressions. No other Pearson correlations had both a $p < 0.05$ and an $R^2 > 0.55$.

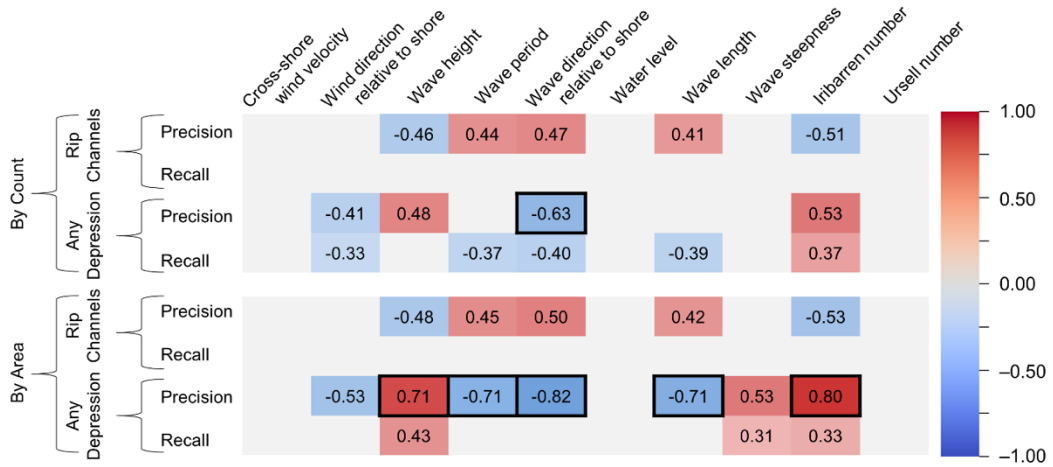

Fig. 7—Heat map of all Pearson correlations. Correlations were calculated between the eight measures of spatial correspondence (left) and the 10 independent variables used to summarize oceanographic conditions during each timex image (top). The top half of the plot shows recall and precision when calculated by count and the bottom half of the plot shows recall and precision when calculated by area. Gray/empty cells indicate relationships with $p > 0.05$. Saturation increased with R2 and six significant relationships ($R^2 > 0.60$) are emphasized with a heavy, black outline. For wind and wave direction relative to shore, lower values indicate forces closer to shore-normal and large values indicate increasingly shore-parallel forces.

3.4.2 Spearman Correlations

When outcomes were tallied by count, there were no significant Spearman rank correlations ($R^2 \geq 0.60$ and $p \leq 0.05$; top half of Fig. 8). However, four variables had a potentially significant correlation ($R^2 \geq 0.55$ and $p \leq 0.05$) with precision for all bathymetric depressions. One of these was negatively correlated and three were positively correlated. As with Pearson correlation by both methods, there was a negative

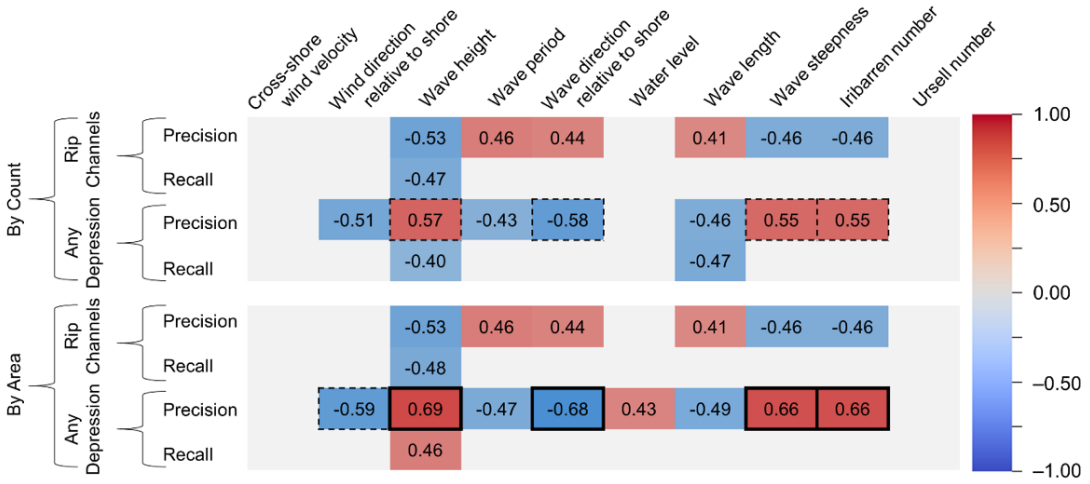

Fig. 8—Heat map of all Spearman rank correlations. Correlations were calculated between the eight measures of spatial correspondence (left) and the10 independent variables used to summarize oceanographic conditions during each timex image (top). Gray/empty cells denote a correlation with $p > 0.05$. The top half of the plot shows rates calculated by count and the bottom half of the plot shows rates calculated by area. Saturation increased with R^2 and four significant relationships ($R^2 > 0.60$) are emphasized with a heavy, black outline. Five potentially significant relationships ($R^2 > 0.55$) have a dashed, black outline. For wind and wave direction relative to shore, lower values indicate forces closer to shore-normal and large values indicate increasingly shore-parallel forces.

correlation between incident wave direction and the precision with which visual signatures indicated all bathymetric depressions (-0.58). Additionally, increased wave height (0.57), increased wave steepness (0.55), and increased Iribarren numbers (0.55) had weakly positive Spearman rank correlation with precision, meaning that these conditions potentially increased the likelihood that a visual signature was a true positive indicator of a bathymetric depression (dashed outlines, top row of Fig. 8). When tallied by count, all other Spearman rank correlations were random or semi-random.

When recall and precision were calculated using the cumulative area within outcomes, four variables were found to have significant correlations with the precision with which visual signatures indicated all bathymetric depressions (bold outlines in bottom half of Fig. 8). One of those relationships was negatively correlated, and three were positively correlated. Again, increasingly oblique incident waves were correlated with decreased precision for all bathymetric depressions (-0.68). Additionally, increasingly shore-parallel winds were weakly correlated with decreased precision for all bathymetric depressions (-0.59). Precision was positively correlated with increased wave heights (0.69), increased wave steepness (0.66), and increased Iribarren numbers (0.66). These are the same relationships correlated when outcomes were tallied by count, but where that method produced Spearman rank correlation values > 0.55, the area method resulted in stronger correlation values > 0.60. Under those conditions, there was an increased likelihood that a visual signature was a true positive for all bathymetric depressions. All other associations were either random or semi-random ($R^2 < 0.55$ and/or $p > 0.05$).

4. DISCUSSION

We evaluated whether visual signatures are reliable indicators of rip channels using timex images created from nearshore camera video imagery and DEMs created from lidar observations. Visual signatures were identified in 51 images captured within ±12 hours of the lidar bathymetry. Analysis was limited to the four dates with lidar observations. The following questions address the motivations for the analysis and context of results.

4.1 Are visual Signatures Consistently Spatially Correspondent to Rip Channels?

Spatial correspondence between visual signatures and rip channels was evaluated with two methods: by count and by area (see summary in Table 3). By all methods of analysis, very few visual signatures indicated a rip channel (2–3%) and > 96% of rip channels were not indicated by visual signatures. In the event that the definition of a rip channel utilized in this study was limiting results, analysis was also extended to the more generally defined set of all bathymetric depressions, which had no restrictions on narrowness or orientation. The results of this analysis indicated that the majority of visual signatures did indicate a bathymetric depression (80–93%) but similar to the results of the rip channel analysis, the majority of all bathymetric depressions were not indicated by visual signatures (92–96%).

Table 3—Summary of Spatial Correspondence Determined by Count and by Area, for Both Sets of Bathymetric Features: Rip Channels and the More Generally Defined "All Bathymetric Depressions"

Metric	All Bathymetric Depressions		Rip channels	
	By Count	By Area	By Count	By Area
Visual signatures that do indicate a bathymetric feature	79.6%	92.8%	3.1%	2.1%
Visual signatures that exist outside of bathymetric features	20.4%	7.2%	96.9%	97.9%
Bathymetric features that are indicated by a visual signature	7.9%	5.9%	3.9%	3.7%
Bathymetric features that exist outside a visual signature	92.1%	94.1%	96.1%	96.3%

These are the same findings shown graphically by Fig. 6. Note that the match between visual signatures and all bathymetric depressions is not a one-to-one relationship; it was possible for more than one visual signature to have spatial correspondence with a large bathymetric depression.

4.2 How Is Spatial Correspondence Affected by Oceanographic Conditions?

The four dates examined in this study represent a range of bathymetric, wind, and wave conditions that are typical of the FRF field site. Pearson and Spearman correlations were used to determine whether oceanographic conditions were correlated with either precision or recall when rip channels were the target, and when all bathymetric depressions were the target. Not all relationships were correlated by both Pearson's linear correlation and Spearman's rank correlation, and the strength of the observed correlations varied depending on whether outcomes were summarized by count or by area. Statistically significant correlations ($R^2 \geq 0.60$) were only found for the precision with which visual signatures indicated all bathymetric depressions. No relationships were found for recall of all bathymetric depressions, or for either recall or precision when rip currents were the target (Table 4).

When rip channels were the target, precision and recall were poor by all methods of analysis. Because recall and precision were always low, regardless of conditions, no statistically significant correlations were found between the oceanographic variables examined and the spatial correspondence of visual signatures with rip channels. When analysis was extended to all bathymetric depressions, several correlations were found. A positive correlation between an oceanographic variable and precision suggests that an increase in that variable is related to an increased likelihood that a visual signature will be a true positive indicator of the target. The precision with which visual signatures indicated all bathymetric depressions was positively

Table 4—Summary Table of Correlations ($p < 0.05$) Found Between Statistics and Oceanographic Variables

Target	Statistic	Method	Variables	Pearson	Spearman
Rip Channels	Recall	Count	*None*		
		Area	*None*		
	Precision	Count	*None*		
		Area	*None*		
All Bathymetric Depressions	Recall	Count	*None*		
		Area	*None*		
	Precision	Count	Wave Height	*None*	0.57
			Wave Direction	-0.63	-0.58
			Wave Steepness	*None*	0.55
			Iribarren Number	*None*	0.55
		Area	Wind Direction	*None*	-0.59
			Wave Height	0.71	0.69
			Wave Direction	-0.82	-0.68
			Wave Period	-0.71	*None*
			Wave Length	-0.71	*None*
			Wave Steepness	*None*	0.66
			Iribarren Number	0.80	0.66
R^2 Value	An increase in the value of the variable is correlated to an increase in the statistic.				
R^2 Value	An increase in the value of the variable is correlated to a decrease in the statistic.				

Colors highlight whether correlations were positive or negative, with more saturated color highlighting $R^2 \geq 0.60$ and less saturated color for $R^2 \geq 0.55$. Wind and wave direction values were degrees from shore-normal, therefore larger values in these categories indicated increasingly shore-parallel forces. Pearson correlation indicates linear relationships. Spearman correlation can indicate nonlinear relationships.

correlated with three variables: wave height (by count, Spearman = 0.57; by area, Pearson = 0.71 Spearman = 0.69), wave steepness (by count, Spearman = 0.55; by area, Spearman = 0.66), and Iribarren number (by count, Spearman = 0.55; by area, Pearson = 0.8 Spearman = 0.66). In contrast, a negative correlation between an oceanographic variable and precision suggests than a decrease in the oceanographic variable is related to an increased likelihood that a visual signature will be a false positive indicator of the target. Precision for all bathymetric depressions was negatively correlated with three variables: increasingly shore normal incident waves (by count, Pearson = -0.63 Spearman = -0.58; by area, Pearson = -0.82 Spearman = -0.68), longer wave periods (by area, Pearson = -0.71), and longer wavelengths (by area, Pearson = -0.71). In addition, there is a possibility that increasingly shore-normal winds are negatively correlated with precision (by area, Spearman = -0.59).

4.3 Do Findings Agree or Conflict with Previous Research?

Our results are in agreement with some of the findings of MacMahan et al. (2005). They measured sediment transport in and around a rip current near Monterey, California, USA, and found that wave heights

affected the reliability of the visual signature as an indicator of a rip channel. They found that pixel intensity in timex images was an acceptable proxy for nearshore bathymetry as long as significant wave height H was > 0.5m and < 2.0 m. They also determined that while some wave breaking was necessary to generate the visual signature (H > 0.5 m), the reliability of the visual signature decreased as H increased beyond a threshold of 2.0 m. Although their aim was not specifically to quantify the reliability of the visual signature as an indicator of bathymetric rip channel presence, they did provide insight into oceanographic effects that may affect the reliability of the visual signature as an indicator of either a rip channel or an actively flowing rip current.

In our study, we observed 0.36 m < H < 1.18 m, with a mean of 0.60 m, which is within the range found by MacMahan et al. (2005) to be associated with true positive visual signatures, and yet we found that visual signatures were a poor indicator of rip channel presence regardless of wave heights, with < 4% of visual signatures correctly indicating a rip channel location. However, when we extended analysis to all bathymetric depressions, our results agreed with the findings of MacMahan et al. (2005). We saw a positive correlation (Pearson R^2 = 0.71, Spearman R^2 = 0.69) where increased wave heights did increase the likelihood that a visual signature would indicate any bathymetric depression, which implies that our definition of a rip channel may have been too restrictive and our definition of a bathymetric channel more consistent with existing literature. We acknowledge, but cannot evaluate, the effects of the differences in bathymetry of the two study sites. MacMahan et al. (2005) observed rip channels along an embayed beach, whereas we observed a relatively straight 1.5 km shoreline at Duck, N.C. It is notable that MacMahan et al. (2005) also included observations of flow in and around the rip channel, which this study does not. Therefore, it is also possible that the spatial correspondence observed by MacMahan et al. (2005) between the visual signatures and rip channels was influenced by the observed offshore-directed flows in the rip channel. They did not analyze spatial correspondence quantitatively, nor separately from flow observations. Therefore, it is possible that the poor correspondence we observed between rip channels and visual signatures was due to a lack of offshore directed flow at the time of our images. Unfortunately, our study did not include in situ observations of flow.

Our results contradict statements from publications that hypothesized that visual signatures may be an optical response to rip channels alone, regardless of rip flow presence (Holman et al., 2003; Konicki and Holman, 2000; Ranasinghe et al., 2004). We found that 96.9% of visual signatures were observed outside of rip channels and 96.1% of rip channels were observed without a visual signature. Expanding analysis to all bathymetric depressions did not resolve this conflict, as 92.1% of all bathymetric depressions existed without a visual signature (Table 3). Notably, Holman et al. (2003) and Ranasinghe et al. (2004) did not include bathymetric data. Konicki and Holman (2000) did include transect surveys that confirmed that transverse bars were spatially coincident with high-intensity pixels, but did not specifically investigate the spatial coincidence of rip channels and low intensity pixels. The advantages provided by the spatially dense lidar bathymetric observations we used here were not available to these earlier studies. It is possible that the relationship between rip channels (regardless of flow) and the visual signature that was proposed in Holman et al. (2003), Konicki and Holman (2000), and Ranasinghe et al. (2004) was limited by the lack of dense bathymetric observations available at the time those studies were conducted.

In addition, field campaigns that observed visual signatures spatially correspondent to rip channels (e.g.: MacMahan et al., 2005; Moulton et al., 2017a) often targeted small regions that were known a priori to have existing rip channels and/or rip currents. Those campaigns were not specifically designed to test the reliability of the visual signature as an indicator of a rip channel presence; therefore, the spatial correspondence observed could be the result of confirmation bias in site selection. In contrast, this study examined a 1.5-km-long nearshore region without a priori knowledge of the bathymetry or of the timing or location of either the visual signature or rip channels. Systematically analyzing this larger region showed that a visual signature can appear outside the target bathymetry, and that the target bathymetry frequently exists without a visual signature.

4.4 Were Results Affected by Methods for Digitizing Features?

We sought to reduce subjectivity by utilizing an automated process to digitize features in both the elevation and imagery datasets. To systematically define the boundaries of a rip channel, we followed the leading method (Brander and Cowell, 2003), which identified all DEM grid cells with elevations below the 5th-order-polynomial trend for the nearshore bathymetry. Those 266 features were referred to in this study as "all bathymetric depressions" but were additionally labeled as rip channels when they were narrow (ratio of offshore extent to alongshore extent > 1.0) and oriented shore-normal ±45°. Rip channels were expected to have high correspondence with the visual signature; however, 96.1% of rip channels were not indicated by visual signatures in imagery. To determine whether the rip channel criteria were too restrictive and thereby limiting the opportunities for spatial correspondence, the 266 features in the "all bathymetric depressions" feature set were also examined for spatial correspondence with visual signatures. That feature set had no restrictions on size, shape, or orientation, and yet 92.1% of those depressions were not indicated by a visual signature. Therefore, we determined that the poor spatial correspondence we observed was not a result of the digitization process used to define bathymetric features.

Previous research identified visual signatures utilizing hand digitization and majority agreement between digitizers (e.g., Ranasinghe et al., 2004) or semi-automated methods (e.g., Splinter et al., 2011). To reduce subjectivity, we identified the visual signatures using the fully automated object identifier developed by Maryan et al. (2019), which was trained with images captured at Duck, North Carolina, USA, and Secret Harbour, WA, Australia. Maryan et al. (2019) found that the object identifier successfully identified 98% of visual signatures present in the dataset they tested. We anticipated that the object identifier was a more objective method for identifying visual signatures than the subjective digitizing by humans (e.g., Ranasinghe et al., 2004; Splinter et al., 2011; and others). However, the machine learner may have had a performance of < 98% recall with the 51 images used in this study.

The object identifier was trained with images coded as true positive (or true negative) by the researchers who developed it, and may reflect their subjective interpretation of a visual signature. Although the object identifier was trained and tested with images of our study site, lighting and surf conditions of our 51 images may have contained differences that impacted the performance of the object identifier. Finally, the object identifier was trained with only visual signature information, and its development was not informed by any bathymetric data. Future research could investigate each of these potential sources of uncertainty. Avenues for further study include retraining the object identifier with a dataset digitized by different researchers, or retraining the object identifier with only those visual signatures known to spatially correspond to a rip channel observed in the bathymetry. These paths forward were beyond the scope of this work, but each is a valid topic for future research.

In summary, both Brander and Cowell (2003) and Maryan et al. (2019) are published and valid methods for automatically and objectively identifying their targets. A sensitivity analysis of feature definition was not the aim of this analysis, but was explored. Results calculated by discrete counts of outcomes and by area did show that spatial correspondence was consistent across multiple methods. Spatial correspondence of visual signatures was poor for both all bathymetric depressions and our definition of a rip channel. Future research may create more precise and accurate methods for digitizing rip channels in bathymetry, and/or for digitizing visual signatures in imagery, but at the time of publication, this study utilized the leading methods available.

4.5 Limitations

The precise and spatially dense observations of lidar for nearshore bathymetry were used to determine the location of bathymetric features. While these data provided high-resolution bathymetry for the entire 1.5-km-long beach, we also had to limit all other analyses to the wind, wave, and bathymetric conditions

during the four 24-hour periods surrounding each lidar survey. Despite this limitation on the date range of analyses, the four DEMs did capture varied beach states, including intermediate states (Wright and Short, 1984) characterized by rip channels in both the 2015 and 2019 DEMs. In addition, the oceanographic conditions on these four dates were typical of the observed beach. Therefore, the dataset included representative conditions of both bathymetry and oceanographic conditions at the site.

There are also limits to the interpretation of correlation statistics. Pearson's correlation uses linear regression to reveal linear relationships between variables. In contrast, Spearman's rank correlation can reveal nonlinear relationships whereby two variables are both increasing or both decreasing, but at different nonlinear rates. These are common statistics in spatial correlation analysis, but nearshore forces do not behave linearly. The relationships between bathymetry, nearshore currents, and waves are dynamically coupled. Using linear regression is a common statistical test to search for influence between variables, but given the nonlinear nature of the 10 oceanographic variables analyzed, it is not surprising to see only six Pearson correlations between precision, recall, and those variables. It is noteworthy that six variables did have Pearson correlations, and that four of those relationships were also significantly correlated in the same direction (and similar magnitude) when analyzed with Spearman's rank correlation (see Table 4). Given that Spearman's rank is not limited to linear relationships, and that nine variables had at least potentially significant relationships to the precision with which visual signatures indicated all bathymetric depressions with these 51 images, it is possible that future analysis of additional images, a greater range of oceanographic conditions, and/or other sites may provide more information with regard to the influence of oceanographic variables on recall and precision. It is also possible that only Spearman's rank is a helpful test for the influence of oceanographic conditions on the reliability of the visual signature as an indicator of rip channels.

4.6 The Visual Signature May Be Caused by Offshore-Directed Flow

Field observations of spatial correspondence between visual signatures and offshore directed flow are often cited as evidence that the visual signature is an indicator of a flowing rip current (Bruneau et al., 2009; MacMahan et al., 2005; Moulton et al., 2017a). Our data did not include observations of flow; therefore, the spatial correspondence between the visual signature and the offshore-directed flow of a rip current could not be analyzed. However, the poor spatial correspondence between bathymetric features and visual signatures we observed does suggest that the visual signature is not generated by bathymetry alone. This finding provides increased support for future research into which oceanographic conditions, including active rip current flow, may cause the visual signature to appear.

5. CONCLUSIONS

The majority of rip channels present in the bathymetry were not indicated by visual signatures identified by the machine learner used here. The same result was observed for the more generally defined target of all bathymetric depressions. The oceanographic conditions that were correlated with precision and recall between the identified visual signature and all bathymetric depressions were consistent with published literature. Additionally, visual signatures were observed over bathymetry that did not meet the definition of a rip channel. Previous studies that utilized visual signatures as indicators of rip channels (or rip currents) have shown that the presence of offshore-directed flow can be spatially correspondent with a visual signature. Future research is needed to investigate how often active rip current flow can be the singular or partial cause of a visual signature, and how often a visual signature is generated by the combination of both offshore directed flow and a bathymetric feature.

REFERENCES

Aarninkhof, S. G. J., & Ruessink, B. G. (2004). Video observations and model predictions of depth-induced wave dissipation. *IEEE Transactions on Geoscience and Remote Sensing*, *42*(11), 2612–2622. https://doi.org/10.1109/TGRS.2004.835349

Almar, R., Cienfuegos, R., Catalán, P. A., Michallet, H., Castelle, B., Bonneton, P., & Marieu, V. (2012). A new breaking wave height direct estimator from video imagery. *Coastal Engineering*, *61*, 42–48. https://doi.org/10.1016/j.coastaleng.2011.12.004

Andriolo, U. (2019). Nearshore Wave Transformation Domains from Video Imagery. *Journal of Marine Science and Engineering*, *7*(6), 186. https://doi.org/10.3390/jmse7060186

Brander, R. W. (1999). Field observations on the morphodynamic evolution of a low-energy rip current system. *Marine Geology*, *157*(3–4), 199–217. https://doi.org/10.1016/S0025-3227(98)00152-2

Brander, R. W., & Cowell, P. J. (2003). A trend-surface technique for discrimination of surf-zone morphology: Rip current channels. *Earth Surface Processes and Landforms*, *28*(8), 905–918. https://doi.org/10.1002/esp.489

Bruneau, N., Castelle, B., Bonneton, P., Pedreros, R., Almar, R., Bonneton, N., Bretel, P., Parisot, J.-P., & Sénéchal, N. (2009). Field observations of an evolving rip current on a meso-macrotidal well-developed inner bar and rip morphology. *Continental Shelf Research*, *29*(14), 1650–1662. https://doi.org/10.1016/j.csr.2009.05.005

Castelle, B., Scott, T., Brander, R. W., & McCarroll, R. J. (2016). Rip current types, circulation and hazard. *Earth-Science Reviews*, *163*, 1–21. https://doi.org/10.1016/j.earscirev.2016.09.008

Chickadel, C. C. (2003). An optical technique for the measurement of longshore currents. *Journal of Geophysical Research*, *108*(C11), 3364. https://doi.org/10.1029/2003JC001774

de Silva, A., Mori, I., Dusek, G., Davis, J., & Pang, A. (2021). Automated rip current detection with region based convolutional neural networks. *Coastal Engineering*, *166*, 103859. https://doi.org/10.1016/j.coastaleng.2021.103859

Gallop, S. L., Bryan, K. R., Coco, G., & Stephens, S. A. (2011). Storm-driven changes in rip channel patterns on an embayed beach. *Geomorphology*, *127*(3–4), 179–188. https://doi.org/10.1016/j.geomorph.2010.12.014

Guedes, R. M. C., Calliari, L. J., Holland, K. T., Plant, N. G., Pereira, P. S., & Alves, F. N. A. (2011). Short-term sandbar variability based on video imagery: Comparison between Time–Average and Time–Variance techniques. *Marine Geology*, *289*(1–4), 122–134. https://doi.org/10.1016/j.margeo.2011.09.015

Haller, M. C. (2002). Experimental study of nearshore dynamics on a barred beach with rip channels. *Journal of Geophysical Research*, *107*(C6), 3061. https://doi.org/10.1029/2001JC000955

Holland, K. T., Holman, R. A., & Sallenger, A. H. (1991). Estimation of overwash bore velocities using video techniques. In *Coastal Sediments* (pp. 489–497). ASCE.

Holman, R. A., & Guza, R. T. (1984). Measuring run-up on a natural beach. *Coastal Engineering*, *8*(2), 129–140. https://doi.org/10.1016/0378-3839(84)90008-5

Holman, R. A., & Stanley, J. (2007). The history and technical capabilities of Argus. *Coastal Engineering*, *54*(6–7), 477–491. https://doi.org/10.1016/j.coastaleng.2007.01.003

Holman, R. A., Symonds, G., Thornton, E. B., & Ranasinghe, R. (2006). Rip spacing and persistence on an embayed beach. *Journal of Geophysical Research*, *111*(C1), C01006. https://doi.org/10.1029/2005JC002965

Holman, R., Plant, N., & Holland, T. (2013). cBathy: A robust algorithm for estimating nearshore bathymetry: The cBathy Algorithm. *Journal of Geophysical Research: Oceans*, *118*(5), 2595–2609. https://doi.org/10.1002/jgrc.20199

Konicki, K. M., & Holman, R. A. (2000). The statistics and kinematics of transverse sand bars on an open coast. *Marine Geology*, *169*(1–2), 69–101. https://doi.org/10.1016/S0025-3227(00)00057-8

Lippmann, T. C., & Holman, R. A. (1989). Quantification of sand bar morphology: A video technique based on wave dissipation. *Journal of Geophysical Research*, *94*(C1), 995. https://doi.org/10.1029/JC094iC01p00995

Lippmann, T. C., & Holman, R. A. (1990). The spatial and temporal variability of sand bar morphology. *Journal of Geophysical Research*, *95*(C7), 11575. https://doi.org/10.1029/JC095iC07p11575

MacMahan, J. H., Thornton, E. B., Stanton, T. P., & Reniers, A. J. H. M. (2005). RIPEX: Observations of a rip current system. *Marine Geology*, *218*(1–4), 113–134. https://doi.org/10.1016/j.margeo.2005.03.019

Mallet, C., Kingston, K. S., Davidson, M. A., & Huntley, D. A. (n.d.). *The use of video in the study of sandbar dynamics*. 6.

Maryan, C., Hoque, M. T., Michael, C., Ioup, E., & Abdelguerfi, M. (2019). Machine learning applications in detecting rip channels from images. *Applied Soft Computing*, *78*, 84–93. https://doi.org/10.1016/j.asoc.2019.02.017

Moulton, M., Elgar, S., Raubenheimer, B., Warner, J. C., & Kumar, N. (2017). Rip currents and alongshore flows in single channels dredged in the surf zone. *Journal of Geophysical Research: Oceans*, *122*(5), 3799–3816. https://doi.org/10.1002/2016JC012222

Orzech, M. D., Thornton, E. B., MacMahan, J. H., O'Reilly, W. C., & Stanton, T. P. (2010). Alongshore rip channel migration and sediment transport. *Marine Geology*, *271*(3–4), 278–291. https://doi.org/10.1016/j.margeo.2010.02.022

Pape, L., Plant, N. G., & Ruessink, B. G. (2010). On cross-shore migration and equilibrium states of nearshore sandbars. *Journal of Geophysical Research*, *115*(F3), F03008. https://doi.org/10.1029/2009JF001501

Piotrowski, C. C., & Dugan, J. P. (2002). Accuracy of bathymetry and current retrievals from airborne optical time-series imaging of shoaling waves. *IEEE Transactions on Geoscience and Remote Sensing*, *40*(12), 2606–2618. https://doi.org/10.1109/TGRS.2002.807578

Quartel, S. (2009). Temporal and spatial behaviour of rip channels in a multiple-barred coastal system. *Earth Surface Processes and Landforms*, *34*(2), 163–176. https://doi.org/10.1002/esp.1685

Ranasinghe, R., Symonds, G., Black, K., & Holman, R. (2004). Morphodynamics of intermediate beaches: A video imaging and numerical modelling study. *Coastal Engineering*, *51*(7), 629–655. https://doi.org/10.1016/j.coastaleng.2004.07.018

Román-Rivera, M. A., & Ellis, J. T. (2019). A synthetic review of remote sensing applications to detect nearshore bars. *Marine Geology*, *408*, 144–153. https://doi.org/10.1016/j.margeo.2018.12.003

Ruessink, B. G., Pape, L., & Turner, I. L. (2009). Daily to interannual cross-shore sandbar migration: Observations from a multiple sandbar system. *Continental Shelf Research*, *29*(14), 1663–1677. https://doi.org/10.1016/j.csr.2009.05.011

Ruessink, B. G., van Enckevort, I. M. J., Kingston, K. S., & Davidson, M. A. (2000). Analysis of observed two- and three-dimensional nearshore bar behaviour. *Marine Geology*, *169*(1–2), 161–183. https://doi.org/10.1016/S0025-3227(00)00060-8

Simarro, G., Bryan, K. R., Guedes, R. M. C., Sancho, A., Guillen, J., & Coco, G. (2015). On the use of variance images for runup and shoreline detection. *Coastal Engineering*, *99*, 136–147. https://doi.org/10.1016/j.coastaleng.2015.03.002

Simarro, G., Calvete, D., Luque, P., Orfila, A., & Ribas, F. (2019). UBathy: A New Approach for Bathymetric Inversion from Video Imagery. *Remote Sensing*, *11*(23), 2722. https://doi.org/10.3390/rs11232722

Splinter, K. D., Holman, R. A., & Plant, N. G. (2011). A behavior-oriented dynamic model for sandbar migration and 2DH evolution. *Journal of Geophysical Research*, *116*(C1), C01020. https://doi.org/10.1029/2010JC006382

Stockdon, H. F., & Holman, R. A. (2000). Estimation of wave phase speed and nearshore bathymetry from video imagery. *Journal of Geophysical Research: Oceans*, *105*(C9), 22015–22033. https://doi.org/10.1029/1999JC000124

Thuan, D. H., Almar, R., Marchesiello, P., & Viet, N. T. (2019). Video Sensing of Nearshore Bathymetry Evolution with Error Estimate. *Journal of Marine Science and Engineering*, *7*(7), 233. https://doi.org/10.3390/jmse7070233

van Enckevort, I. M. J., & Ruessink, B. G. (2001). Effect of hydrodynamics and bathymetry on video estimates of nearshore sandbar position. *Journal of Geophysical Research: Oceans*, *106*(C8), 16969–16979. https://doi.org/10.1029/1999JC000167

Wright, L.D., & Short, A.D. (1984). Morphodynamic variability of surf zones and beaches: A synthesis, Marine Geology, 56(1–4), 93-118. https://doi.org/10.1016/0025-3227(84)90008-2